Talanta 82 (2010) 516–522

Contents lists available at ScienceDirect

Talanta

journal homepage: www.elsevier.com/locate/talanta

# A label-free colorimetric detection of lead ions by controlling the ligand shells of gold nanoparticles

Yu-Lun Hung [a], Tung-Ming Hsiung [a], Yi-You Chen [a], Chih-Ching Huang [a,b,*]

[a] Institute of Bioscience and Biotechnology, National Taiwan Ocean University, 2 Beining Road, Keelung 20224, Taiwan
[b] Center for Marine Bioenvironment and Biotechnology, National Taiwan Ocean University, 2 Beining Road, Keelung 20224, Taiwan

ARTICLE INFO

*Article history:*
Received 19 March 2010
Received in revised form 6 May 2010
Accepted 7 May 2010
Available online 13 May 2010

*Keywords:*
Lead ions
Gold nanoparticles
Ligand shell
Label-free
Colorimetric detection

ABSTRACT

We have developed a simple, colorimetric and label-free gold nanoparticle (Au NP)-based probe for the detection of $Pb^{2+}$ ions in aqueous solution, operating on the principle that $Pb^{2+}$ ions change the ligand shell of thiosulfate ($S_2O_3^{2-}$)-passivated Au NPs. Au NPs reacted with $S_2O_3^{2-}$ ions in solution to form $Au^+ \cdot S_2O_3^{2-}$ ligand shells on the Au NP surfaces, thereby inhibiting the access of 4-mercaptobutanol (4-MB). Surface-assisted laser desorption/ionization time-of-flight ionization mass spectrometry (SALDI–TOF MS) and inductively coupled plasma mass spectrometry (ICP-MS) measurements revealed that PbAu alloys formed on the surfaces of the Au NPs in the presence of $Pb^{2+}$ ions; these alloys weakened the stability of the $Au^+ \cdot S_2O_3^{2-}$ ligand shells, enhancing the access of 4-MB to the Au NP surfaces and, therefore, inducing their aggregation. As a result, the surface plasmon resonance (SPR) absorption of the Au NPs red-shifted and broadened, allowing quantitation of the $Pb^{2+}$ ions in the aqueous solution. This 4-MB/$S_2O_3^{2-}$–Au NP probe is highly sensitive (linear detection range: 0.5–10 nM) and selective (by at least 100-fold over other metal ions) toward $Pb^{2+}$ ions. This cost-effective sensing system allows the rapid and simple determination of the concentrations of $Pb^{2+}$ ions in real samples (in this case, river water, Montana soil and urine samples).



## 1. Introduction

Lead (Pb) is one of the most toxic metallic pollutants that affect virtually every system in the body. Even exposure to very low levels of Pb (<100 μg/L in blood) can cause neurological, reproductive, cardiovascular, and developmental disorders [1–7]. Children are more vulnerable to lead exposure than adults because of higher rate of intestinal absorption and retention and of variants in iron metabolism genes that may be more susceptible to Pb absorption and accumulation. The concentrations of Pb present in environmental and biological samples generally vary from the parts-per-billion to the parts-per-million level, suggesting the need for very sensitive analytical techniques [3]. Several methods for Pb analysis have been developed in the last decade, including classical atomic absorption/emission spectrometry, inductively coupled plasma mass spectrometry (ICP-MS), thermal ionization mass spectrometry (TIMS), X-ray fluorescence spectrometry (XRF), anodic stripping voltammetry and reversed-phase high-performance liquid chromatography coupled with UV–vis or fluorescence detection [3]. These methods are sensitive and accurate for determination of Pb, but they are time-consuming, expensive, and/or require sophisticated equipment. Thus, a simple and inexpensive method for quantifying the levels of Pb in environmental, biological, and industrial samples remains desirable.

Fluorescence probes, for examples using fluorescent chromophores [8–14], DNA [15–21], polymers [22], and proteins [23–26] have been demonstrated for the selective detection of $Pb^{2+}$ ions in aqueous solutions. But these probes have limited practical use because of, for example, poor aqueous solubility, cross-sensitivity toward other metal ions, matrix interference, high cost, complicated processing, the need for unstable molecules, and/or poor sensitivity. Ideally, a cost-effective and simple method for rapid quantitation of $Pb^{2+}$ ions would involve simple colorimetric detection; the signaling of the targeted event occurs through a visual color change in the reaction medium [27–29]. In some cases, chromophore-based sensors for the detection of $Pb^{2+}$ is however not sensitive enough [28,29].

Thiol-functionalized gold nanoparticles (Au NPs) are interesting nanomaterials for use as colorimetric reporters because of their small sizes, large surface-area-to-volume ratios, long-term stability, compatibility with biomolecules, and unique optical properties, including extremely high extinction coefficients ($10^8$ to $10^{10}$ $M^{-1}$ $cm^{-1}$) of their surface plasmon resonance (SPR) absorptions, strongly distance-dependent optical properties, and efficient

* Corresponding author at: Institute of Bioscience and Biotechnology, National Taiwan Ocean University, 2 Beining Road, Keelung 20224, Taiwan.
Tel.: +886 2 24622192x5517; fax: +886 2 2462 2320.
*E-mail address:* huanging@ntou.edu.tw (C.-C. Huang).

0039-9140/$ – see front matter © 2010 Elsevier B.V. All rights reserved.
doi:10.1016/j.talanta.2010.05.004

quenching characteristics [30–34]. The extinction cross-sections of Au NPs and the wavelengths at which they absorb and scatter light depend on their sizes and shapes, the dielectric properties (refractive index) of the surrounding medium, and their interactions with neighboring particles [30–34]. Systems based on analyte-induced aggregation of Au NPs have been employed for the colorimetric detection of cells, viruses, nucleic acids, proteins, small molecules, and metal ions [35–39]. For examples, Au NPs functionalized with gallic acid, 11-mercaptoundecanoic acid, and peptides have all been demonstrated separately for the selective detection of $Pb^{2+}$ ions [40–43]. Alternately, a colorimetric $Pb^{2+}$ sensor was developed using 17E DNAzyme and Au NPs [44]. This colorimetric method required several steps, including modifying the DNAzyme (or its substrate) onto the Au NPs. The substrate strand of a DNAzyme extended at both termini was used to aggregate the Au NPs: in the absence of $Pb^{2+}$ ions, the Au NPs remained aggregated, displaying a purple color; in their presence, the aggregates were dispersed through a $Pb^{2+}$-specific cleavage reaction, resulting in a red color. These steps complicate and increase the cost of performing such experiments. Simple, sensitive, and label-free DNAzyme-based sensors for $Pb^{2+}$ detection using unmodified Au NPs have been developed by taking advantage of the fact that unfolded single-stranded (ss)DNA binds more strongly to citrate-protected Au NPs than does double-stranded (ds)DNA [45,46]. Nevertheless, these probes require the expensive DNAzyme, exhibit interference from other divalent metal ions, and sense $Pb^{2+}$ ions only in buffer solutions.

Previously, we have developed a colorimetric and nonaggregation-based Au NPs probe for the detection of $Pb^{2+}$ in aqueous solution, based on the fact that $Pb^{2+}$ ions accelerate the leaching rate of Au NPs by thiosulfate ($S_2O_3^{2-}$) and 2-mercaptoethanol (2-ME) [27]. The developed 2-ME/$S_2O_3^{2-}$–Au NP probe was selective detection of $Pb^{2+}$ to nM without a need of using complicated chemosensors or sophisticated equipment [27]. However, because of the leaching of Au NPs was involved oxidation of Au NPs and, thus, the sensing was highly time-depended and interfered by foreign oxidant, reductant, heavy metallic ions and ligands. To overcome these shortcomings, we developed a label-free, rapid, and homogeneous assay – employing Au NPs, $S_2O_3^{2-}$, and 4-mercaptobutanol (4-MB) – for the highly selective and sensitive detection of $Pb^{2+}$ ions in this study. Alternately, this new approach was based on the control of ligand shells of Au NPs, which was not interfered by foreign oxidants and reductants and it thus showed highly selective toward $Pb^{2+}$ ions. We also demonstrate the practicality of this approach for the determination of $Pb^{2+}$ in river water, soil and as well as complicated biological urine samples.

## 2. Materials and methods

### 2.1. Chemicals

4-Mercaptobutanol (4-MB), 6-mercaptohexanol (6-MH), 9-mercaptononanol (9-MN), 2-mercaptoacetic acid (2-MAA), 3-mercaptopropionic acid (3-MPA), sodium thiosulfate, trisodium citrate, glycine, and all metal salts were purchased from Aldrich (Milwaukee, WI). Hydrogen tetrachloroaurate(III) trihydrate was obtained from Acros (Geel, Belgium). Montana Soil (SRM 2710) and urine (SRM 2672a) were obtained from the National Institute of Standards and Technology (NIST, Maryland). Milli-Q ultrapure water was used in each experiment. The buffer was 50 mM glycine solution (pH 8–10, adjusted with 1.0N NaOH).

### 2.2. Synthesis of 14.2-nm spherical Au NPs

The 14.2-nm spherical Au NPs were prepared through citrate-mediated reduction of $HAuCl_4$ [47]. Aqueous 1 mM $HAuCl_4$ (250 mL) was brought to a vigorous boil while stirring in a round-bottom flask fitted with a reflux condenser; 38.8 mM trisodium citrate (25 mL) was added rapidly to the solution, which was heated for another 15 min, during which time its color changed from pale yellow to deep red. The solution was cooled to room temperature with continuous stirring.

### 2.3. Characterization of Au NPs

Transmission electron microscope (TEM) images of Au NPs were recorded using an H7100 transmission electron microscope (Hitachi High-Technologies Corporation, Tokyo, Japan) operated at 125 kV. Samples for TEM measurements were prepared by placing a drop (20 μL) of the Au NP solution on a carbon-coated copper grid and then drying at room temperature. The sizes of the Au NPs were verified through TEM analysis, they appeared to be nearly monodisperse, with an average size of $14.2 \pm 0.3$ nm (1000 counts). A double-beam UV–vis spectrophotometer (Cintra 10e, GBC, Victoria, Australia) was used to measure the absorption of the Au NP solution. The particle concentration of the Au NPs (15 nM) was determined according to Beer's law using an extinction coefficient of ca. $2.43 \times 10^8\ M^{-1}\ cm^{-1}$ at 520 nm for the 14.2-nm Au NPs [27,47]. The zeta potentials of the Au NPs were measured using a Zetasizer 3000HS analyzer (Malvern Instruments, Malvern, U.K.). For surface-assisted laser desorption/ionization time-of-flight ionization mass spectrometry (SALDI–TOF MS) measurements, aliquots (1.0 mL) of the 4-MB/$S_2O_3^{2-}$–Au NPs (1.5 nM) were equilibrated in the absence and presence of $Pb^{2+}$ (10 μM) for 60 min at ambient temperature and then subjected to centrifugation at RCF $35{,}000 \times g$ for 20 min. Following removal of the supernatants, the precipitates were washed with water. After three centrifugation/washing cycles, the pellets were resuspended in water. A portion of each sample (ca. 1.0 μL) was cast onto a stainless-steel 96-well MALDI target and dried in air at room temperature prior to SALDI-TOF MS measurement. The samples were irradiated with a 337-nm nitrogen laser at 10 Hz. Ions produced by laser desorption were stabilized energetically during a delayed extraction period of 200 ns and then accelerated through the TOF system in the reflection mode prior to entering the mass analyzer. Positive ions were detected over a *m/z* range from 1–4 kDa. To obtain high resolution and high S/N ratios, the laser fluence was adjusted to slightly higher than the threshold and each mass spectrum was generated by averaging 300 laser pulses.

### 2.4. 4-MB/$S_2O_3^{2-}$–Au NP-based sensor for $Pb^{2+}$ ions

Aliquots (490 μL) of 5 mM glycine–NaOH (pH 10.0) solutions containing the Au NPs (1.5 nM), $Na_2S_2O_3$ ($10^{-5}$ M), NaCl (15 mM) and $Pb^{2+}$ ions (0–25 nM) were equilibrated at room temperature for 0.5 h. 4-MB (50 mM, 10 μL) was added to each of these mixtures, which were then equilibrated through gentle shaking at room temperature for other 1.5 h. The mixtures were then transferred separately into 96-well microtiter plates and their UV–vis absorption spectra were recorded using a μ-Quant microplate reader (Biotek Instruments, Winooski, VT, USA). The final concentrations of the species are provided herein. As controls, 2-ME, 6-MH, 9-MN, 2-MAA, and 3-MPA instead of 4-MB were added to the mixtures containing Au NPs, $Na_2S_2O_3$, NaCl, and $Pb^{2+}$ ions.

### 2.5. Analysis of water, soil and urine samples

A water sample collected from a river on the campus of National Taiwan Ocean University (NTOU) was filtered through a 0.2-μm membrane. Aliquots of the river water (250 μL) were spiked with standard $Pb^{2+}$ solutions (10 μL) at concentrations ranging from 0 to 25 nM. The spiked samples were then diluted to 500 μL with solu-

tions containing the 4-MB/$S_2O_3^{2-}$–Au NP (1.5 nM) probe, 15 mM NaCl, and 5 mM glycine–NaOH (pH 10.0). The spiked samples were then analyzed separately using ICP-MS and the developed sensing technique.

Acidic digestion of soil samples was performed according to EPA method 305B [48,49]. A soil sample (SRM 2710; 0.01 g) was weighed in an Erlenmeyer flask and $HNO_3$:water (1:1, v/v; 10 mL) was added. The solution was heated on a hot plate to ca. 95 °C (i.e., without boiling) and maintained at this temperature for 15 min. After cooling to less than 70 °C, concentrated $HNO_3$ (5 mL) was added and then the sample was heated under reflux for 30 min at ca. 95 °C without boiling. This step was repeated a second time. The sample was evaporated to ca. 5 mL without boiling. After cooling to less than 70 °C, 18-MΩ water (2 mL) was added, followed by the slow addition of $H_2O_2$ (30%, 10 mL); care was taken to ensure that losses did not occur as a result of the excessive vigorous effervescence caused by rapidly adding this strong oxidant. The solution was then heated until effervescence subsided. After cooling to less than 70 °C, concentrated HCl (5 mL) and 18-MΩ water (10 mL) were added and then the sample was heated under reflux for 15 min without boiling. After cooling to room temperature, the sample was filtered and diluted to 100 mL using DI water. The aqueous soil sample (0.08 mL) was further diluted with DI water to 100 mL. Aliquots (250 μL) of the diluted solutions were spiked with standard $Pb^{2+}$ solutions (10 μL) at concentrations ranging from 0 to 3 nM. The spiked samples were then diluted to 500 μL with solutions containing the 4-MB/$S_2O_3^{2-}$–Au NP (1.5 nM) probe, 15 mM NaCl, and 5 mM glycine–NaOH (pH 10.0).

A urine sample (SRM 2672a) was filtered through a 0.2 μm membrane. Aliquots of the urine sample (980 μL) were spiked with standard $Pb^{2+}$ solutions (20 μL) at concentrations ranging from 0 to 15 nM. The spiked samples were then diluted to 500 μL with solutions containing the 4-MB/$S_2O_3^{2-}$–Au NP (1.5 nM) probe, 15 mM NaCl, and 5 mM glycine–NaOH (pH 10.0). The spiked samples were then analyzed separately using ICP-MS and the developed sensing technique.

## 3. Results and discussion

### 3.1. Mechanism for $Pb^{2+}$-induced aggregation of Au NPs

Scheme 1 reveals that the Au NPs reacted with $S_2O_3^{2-}$ ions in solution to form $Au^+ \cdot S_2O_3^{2-}$ complexes immediately on the Au NP surfaces, resulting in changes of the refractive index of particle's surrounding medium and thus leading to slight changes in their SPR absorption. After adding $Pb^{2+}$ ions and 4-MB, the Au NPs rapidly aggregated in solution. As a result, the SPR absorption band red-shifted dramatically, allowing quantitation of the $Pb^{2+}$ ions in the aqueous solution. The dispersed Au NPs (14.2 ± 0.3 nm) displayed an extinction band (extinction coefficient: $2.43 \times 10^8\ M^{-1}\ cm^{-1}$) at 520 nm; upon aggregation, the signal underwent a red shift with decreased extinction, while the intensity of the signal at 650 nm increased. The extinction coefficients at 650 and 520 nm are related, respectively, to the quantities of the dispersed and aggregated Au NPs. Thus, we used $Ex_{650/520}$, the ratio of the extinction values at these two wavelengths, to express the molar ratio of the aggregated and dispersed Au NPs [35–39]. Fig. 1 displays the $Ex_{650/520}$ ratios of Au NPs (1.5 nM) in 5 mM glycine–NaOH buffer (pH 10) containing sodium thiosulfate ($Na_2S_2O_2$; 0–$1 \times 10^{-3}$ M) and 4-MB ($1 \times 10^{-6} - 1 \times 10^{-3}$ M) in the absence and presence of $PbCl_2$ (1.0 or 10 μM). We note that 4-MB (≥$10^{-5}$ M) induced a large degree of aggregation among the Au NPs that had not been pretreated with $Na_2S_2O_3$ (Fig. 1A). The zeta potentials of the Au NPs in the absence and presence of $10^{-5}$ M $Na_2S_2O_3$ solution were −23.8 and −37.7 mV, respectively. The more-negative zeta potential of the latter supports the notion that $S_2O_3^{2-}$ ions were bound to the surfaces of the Au NPs. The negative zeta potential of the non-passivated Au NPs decreased dramatically to −7.6 mV in the presence of 4-MB ($1 \times 10^{-5}$ M), presumably because of the formation of Au NPs aggregates. In contrast, the zeta potential decreased only slightly to −21.3 mV for the $S_2O_3^{2-}$ ($1 \times 10^{-5}$ M)-passivated Au NPs in the presence of 4-MB ($1 \times 10^{-5}$ M). Thus, it was more difficult for 4-MB to access and to bind to the surfaces of the $S_2O_3^{2-}$-passivated Au NPs. We note that the sensing strategy (4-MB induced aggregation) in this study is different from our previous developed 2-ME/$S_2O_3^{2-}$–Au NPs nanosensor, which was based on 2-ME induced oxidation and subsequent leaching of Au NPs [27].

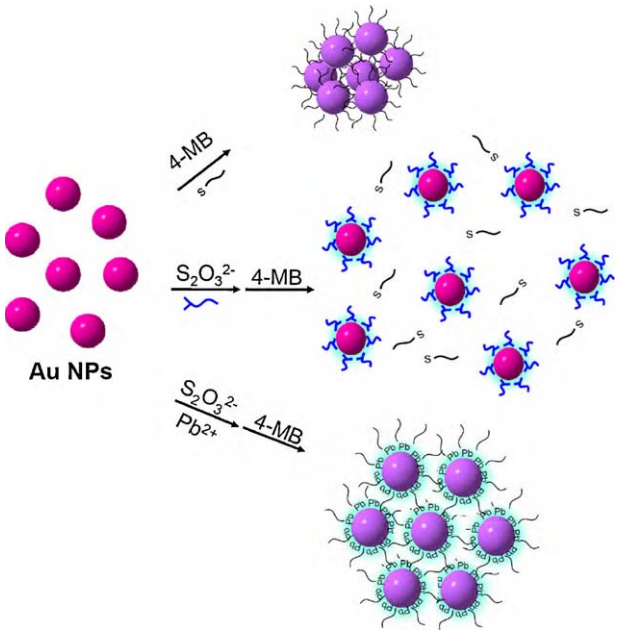


**Scheme 1.** Cartoon representation of the sensing mechanism of the 4-MB/$S_2O_3^{2-}$–Au NP probe for the detection of $Pb^{2+}$ ions.

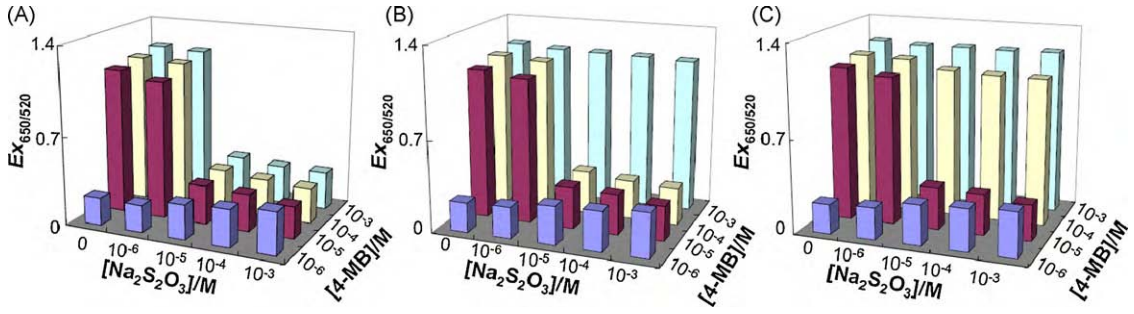


**Fig. 1.** Values of the $Ex_{650/520}$ ratios of the 4-MB/$S_2O_3^{2-}$–Au NP solutions in the (A) absence and (B and C) presence of (B) 1.0 μM and (C) 10 μM $PbCl_2$. Concentrations: Au NPs, 1.5 nM; $Na_2S_2O_3$, from 0 to $1 \times 10^{-3}$ M; 4-MB, from $1 \times 10^{-6}$ to $1 \times 10^{-3}$ M. Buffer: 5 mM glycine–NaOH (pH 10.0).

Several studies were performed to examine how various metal ions (e.g., $Pb^{2+}$, $Ag^{+}$, $Hg^{2+}$, $Tl^{3+}$, and $Bi^{2+}$) affect the surface properties of Au in the presence of various complexing ligands (e.g., $CN^{-}$, $HS^{-}$, and $S_2O_3^{2-}$) [50–55]. In this present study, we observed that $Pb^{2+}$ ions induced the aggregation of Au NPs in the 4-MB/$S_2O_3^{2-}$–Au NP system. For example, concentrations of $Pb^{2+}$ ions of 1.0 μM (Fig. 1B) and 10 μM (Fig. 1C) induced aggregations of $S_2O_3^{2-}$ ($\geq 10^{-5}$ M)-passivated Au NPs in the presence of 4-MB at concentrations of $1 \times 10^{-3}$ M and from $1 \times 10^{-4}$ to $1 \times 10^{-3}$ M, respectively. In the presence of $S_2O_3^{2-}$, $Pb^{2+}$ ions reacted with Au atoms to form $AuPb_2$ and $AuPb_3$ alloys or metallic Pb on the Au surface, thereby changing the stability of the $S_2O_3^{2-}$-passivating layer. $S_2O_3^{2-}$ is a divalent-type soft ligand that tends to form stable complexes with low-spin $d^{10}$ $Au^{+}$ ions {$\log \beta[Au(S_2O_3)_2^{3-}]$ = ca. 26} [56]. In contrast, the smaller stability constant {$\log \beta[Pb(S_2O_3)_4^{6-}]$ = ca. 7.3} for $Pb(S_2O_3)_4^{6-}$ species suggests that they are much less stable than $Au(S_2O_3)_2^{3-}$ species on Au NP surfaces. As a result, 4-MB molecules can readily access and bind to the surfaces of $S_2O_3^{2-}$-passivated Au NPs in the presence of $Pb^{2+}$. When neutral charged 4-MB accessed to the surfaces of the Au NPs, displacing the citrate ions through the formation of stronger Au–S linkages (bond energy: ca. 184 kJ $mol^{-1}$), leading to reduced the surface charge density and thereby inducing aggregation. On the other hand, when negatively charged thiols, such 2-MAA and 3-MPA were bound to the $S_2O_3^{2-}$–Au NPs in the presence of $Pb^{2+}$ ions, the surface charged density did not change significantly. As a result, the $S_2O_3^{2-}$–Au NPs were stable. We observed similar results (data not shown) for the $Pb^{2+}$ (1.0 μM)-induced aggregation of $S_2O_3^{2-}$ ($\geq 10^{-5}$ M)-passivated Au NPs in the presence of 6-MH ($\geq 10^{-4}$ M) and 9-MN ($\geq 10^{-6}$ M). The longer alkanethiol chains of 6-MH and 9-MN increased the hydrophobicity, resulting in decreases in the solubility and inducing larger degree of aggregation of the thiolate–Au NPs in aqueous solution; therefore, these two thiols at lower concentrations relative to that of 4-MB-induced aggregation of the $S_2O_3^{2-}$–Au NPs in the presence of $Pb^{2+}$ ions. Previously, we found that $Pb^{2+}$-induced leaching of $S_2O_3^{2-}$ ($\geq 10^{-3}$ M)-passivated Au NPs in the presence of 2-mercaptoethanol (2-ME; $\geq 10^{-4}$ M) [27]. The shorter alkanethiol chain of 2-ME increased the solubility of the Au–thiolate complexes in aqueous solution; therefore, 2-ME induced strong leaching [27]. The longer chain length of alkanethiol increased the hydrophobicity on the surfaces of the $S_2O_3^{2-}$–Au NPs and the solubility of the thiolate–Au complexes was lower. As a result, 4-MB, 6-MH and 9-MN induced aggregation instead of leaching of the $S_2O_3^{2-}$–Au NPs in the presence of $Pb^{2+}$ ions.

### 3.2. Evidence of the formation of Pb–Au alloys

Similar to our previous report [27], we used ICP-MS and SALDI-TOF MS to demonstrate the formation of Au–Pb alloys on the surfaces of Au NPs. ICP-MS was used to quantitatively determine the content of Pb formed on the Au NPs in the presence of 4-MB ($1 \times 10^{-3}$ M), $S_2O_3^{2-}$ ($1 \times 10^{-5}$ M), and $Pb^{2+}$ (10 μM). We estimated that 483 Pb atoms/Au NP were present in the precipitate. In addition, we took advantage of high reproducibility and high throughput of SALDI–TOF MS and its simple sample preparation to prove that PbAu alloys formed on the surfaces of the Au NPs [57]. In the SALDI-MS method, photoabsorption by Au NPs induces the desorption and ionization of surface atoms. Fig. S1A reveals the presence of cationic clusters of the type $[Au_n]^{+}$ ($n$ = 6–20) that indicate the fragmentation/vaporization of the Au NPs. Fig. S1B presents mass spectra of the 4-MB ($10^{-3}$ M)/$S_2O_3^{2-}$ ($10^{-5}$ M)–Au NPs in the presence of $Pb^{2+}$ ions (10 μM). We assign the peaks at $m/z$ 1969.67–2024.72 (insets to Fig. S1B) to $[Au_{10-n}Pb_n]^{+}$ ions, where n is an integer ranging from 0 to 5. These $[Au_{10-n}Pb_n]^{+}$ signals are strong evidence for the formation of $Au_{m-n}Pb_n$ alloys on the Au NPs surfaces.

### 3.3. Optimization of the sensing system

Having observed that $Pb^{2+}$ induced the aggregation of Au NPs in the presence of 4-MB and $S_2O_3^{2-}$, we suspected that the sensitivity of our analytical system would be dependent on the pH and salt concentration. Fig. 2A displays the effect of pH on the aggregation of Au NPs in the 4-MB/$S_2O_3^{2-}$–Au NPs system in the presence of various concentrations of $Pb^{2+}$ ions (0–10 μM). From the calibration curves of $Pb^{2+}$ in various glycine–NaOH buffers (pH 8–12), we found that the value of $Ex_{650/520}$ of 4-MB/$S_2O_3^{2-}$–Au NPs solution, in the presence of $Pb^{2+}$ ions, increased upon increasing the pH. Molecules of 4-MB have more ready access for binding to the surfaces of Au NPs at values of pH greater than its $pK_a$ (8.8–9.1), thereby facilitating the aggregation of the Au NPs [58]. We note that the detection dynamic range of our probe for $Pb^{2+}$ was tunable by varying pH values. For example, the detection dynamic ranges were 10–100 nM and 100 nM–250 μM at pH values of 12.0 and 9.0, respectively. A tunable dynamic range is important for practical applications as the desirable concentrations for the same target analyte can be different for various applications [46]. Although the 4-MB/$S_2O_3^{2-}$–Au NP solution at pH 12 provided the best sensitivity for the detection of $Pb^{2+}$ ions, the linear range (10–100 nM) was narrow. When using a solution of the 4-MB/$S_2O_3^{2-}$–Au NPs at pH 10.0, we obtained a wide linear range for the detection of $Pb^{2+}$ ions: from 10 nM to 1.0 μM.

At pH 10.0, we investigated the effect of salt on the sensitivity of the detection of $Pb^{2+}$ using 4-MB/$S_2O_3^{2-}$–Au NPs. Upon increasing the NaCl concentration, salt screening reduced the surface charge density of the $S_2O_3^{2-}$-passivated Au NPs, leading to 4-MB more readily inducing the aggregation of the Au NPs. Fig. 2B indicates that, in the absence of $Pb^{2+}$ ions, the 4-MB/$S_2O_3^{2-}$–Au NPs aggregated at NaCl concentrations greater than 25 mM. The optimal conditions for sensing $Pb^{2+}$ ions were the use of a 5 mM glycine–NaOH solution (pH 10.0) containing 4-MB/$S_2O_3^{2-}$–Au NPs

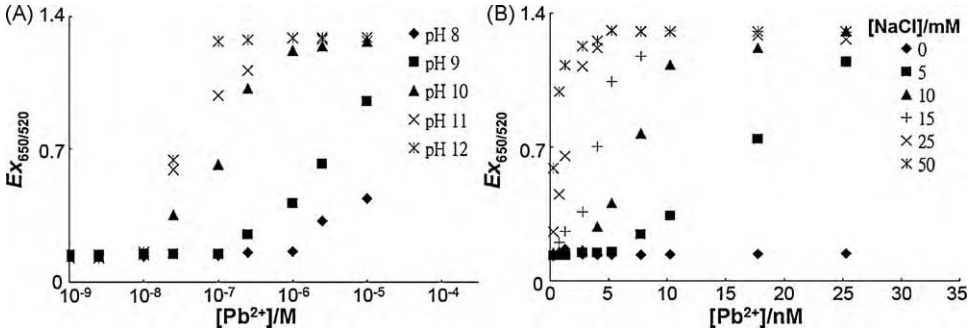


**Fig. 2.** Effect of the (A) pH (8–12) and (B) concentration of NaCl (0–50 mM) on the values of $Ex_{650/520}$ of the 4-MB/$S_2O_3^{2-}$–Au NP (1.5 nM) solutions in the presence of 0–10 μM or 0–25 nM $PbCl_2$, respectively.

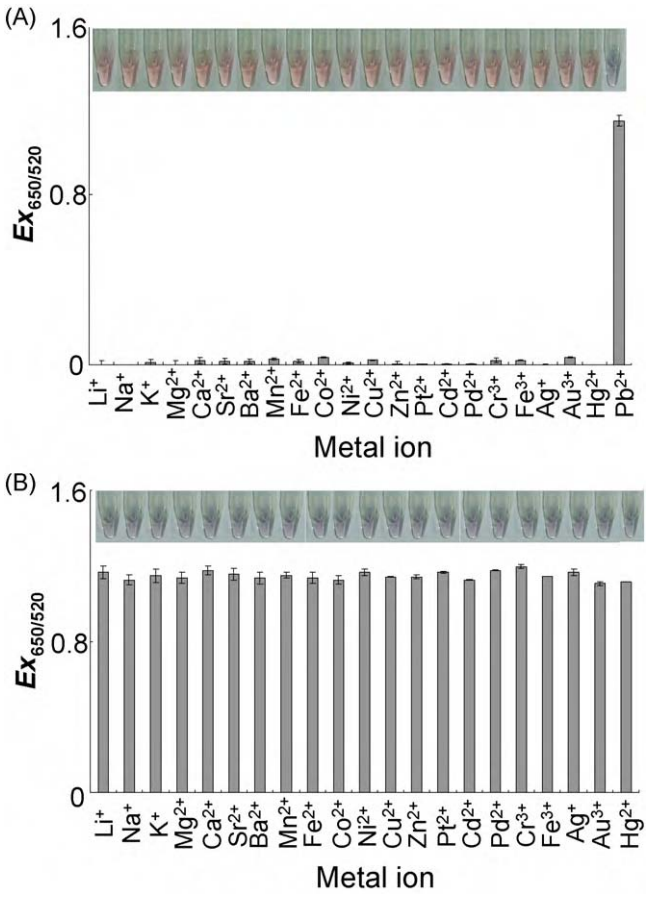


**Fig. 3.** (A) Selectivity of the 4-ME/$S_2O_3^{2-}$–Au NP (1.5 nM) probe toward $Pb^{2+}$ ions (10 nM) against to other metal ions (1.0 μM each). (B) Values of $Ex_{650/520}$ for solutions of 4-MB/$S_2O_3^{2-}$–Au NPs (1.5 nM) in 5 mM glycine–NaOH (pH 10.0) containing 15 mM NaCl and 10 nM $PbCl_2$ in the absence or presence of 100 nM background metal ions. Insets: Photographic images of the Au NP solutions. Error bars represent standard deviations from four repeated experiments.

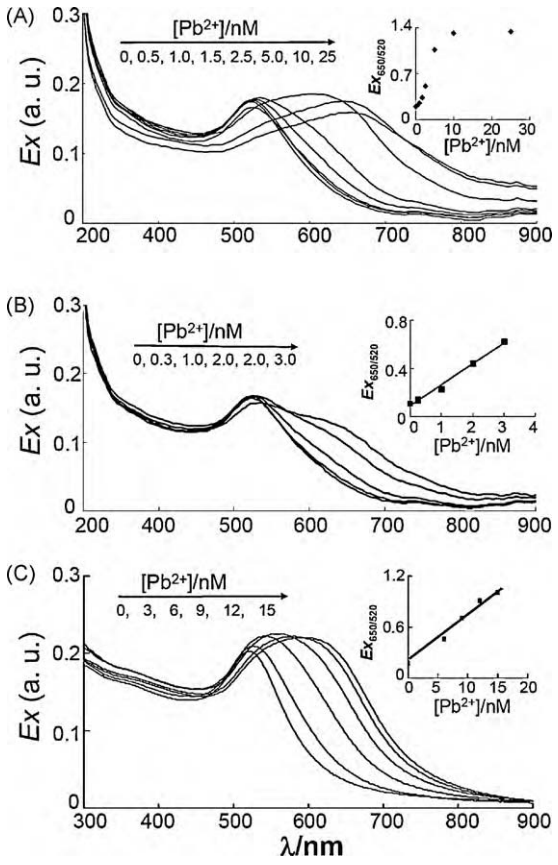


**Fig. 4.** Analyses of representative (A) river water, (B) soil and (C) urine samples using the 4-MB/$S_2O_3^{2-}$–Au NP (1.5 nM) probe. The samples were spiked with $Pb^{2+}$ ions at concentrations of (A) 0–25 nM, (B) 0–3 nM and (C) 0–15 nM. The extinctions (*Ex*) are plotted in arbitrary units (a. u.).

(1.5 nM) and 15 mM NaCl. Upon increasing the concentration of the $Pb^{2+}$ ions, the value of the ratio $Ex_{650/520}$ increased. A linear correlation ($R^2$ = 0.96) existed between the value of $Ex_{650/520}$ and the concentration of $Pb^{2+}$ over the range from 0.5 to 10 nM. The limit of detection (LOD) for $Pb^{2+}$ was 0.2 nM [signal-to-noise (S/N) ratio = 3], much lower than the maximum level (75 nM) of Pb permitted by the United States Environmental Protection Agency (EPA) for drinking water [4]. This approach provides a sensitivity that is one order of magnitude lower than that reported for an aggregation-mediated colorimetric Au NP-based heavy metal ion sensor [40–46].

### 3.4. Selectivity

Because our 4-MB/$S_2O_3^{2-}$–Au NPs allowed the detection of $Pb^{2+}$ ions at concentrations as low as 0.2 nM, we tested the sensor's selectivity by further investigating the changes in the values of $Ex_{650/520}$ of the 4-MB/$S_2O_3^{2-}$–Au NPs (1.5 nM) in the presence of $Na_2S_2O_3^{2-}$ ($10^{-5}$ M), 4-MB ($10^{-3}$ M), $Pb^{2+}$ (10 nM), and an additional metal ion [$Li^+$, $Na^+$, $K^+$, $Mg^{2+}$, $Ca^{2+}$, $Sr^{2+}$, $Ba^{2+}$, $Mn^{2+}$, $Fe^{2+}$, $Co^{2+}$, $Ni^{2+}$, $Cu^{2+}$, $Zn^{2+}$, $Pt^{2+}$, $Cd^{2+}$, $Pd^{2+}$, $Cr^{3+}$, $Fe^{3+}$, $Ag^+$, $Au^{3+}$, or $Hg^{2+}$ (1.0 μM)]. As indicated in Fig. 3A, our system responded selectively toward $Pb^{2+}$ ions – by a factor of 100-fold or more – relative to the other metal ions. The tolerable concentrations of these metal ions for the sensing of $Pb^{2+}$ ions when using this approach were at least 10 times higher than the $Pb^{2+}$ concentration (Fig. 3B). Although, Hg also easily to formation Au–Hg alloys on the Au NPs. The stronger affinity of alkanethiols {$\log \beta[Hg(SR)_2]$ = ca. 45} and $S_2O_3^{2-}$ {$\log \beta[Hg(S_2O_3^{2-})_3^{4-}]$ = ca. 31} toward $Hg^{2+}$ ions result in the formations of stable 4-MB–$Hg^{2+}$ and $S_2O_3^{2-}$–$Hg^{2+}$ complexes in the bulk solution, and, thereby inhibiting formation of Hg–Au alloys on the surfaces of the $S_2O_3^{2-}$–Au NPs. Our reasoning was supported by the SALDI-MS and ICP-MS data, no Hg species were detected. We note that relative to the 4-MB/$S_2O_3^{2-}$–Au NPs probe, our previous 2-ME/$S_2O_3^{2-}$–Au NPs probe was less selective; it was interfered by foreign oxidants and reductants. For example, the 2-ME/$S_2O_3^{2-}$–Au NPs was lower sensitive for detection of $Pb^{2+}$ in the presence of $H_2O_2$ (100 μM). On the contrast, the present 4-MB/$S_2O_3^{2-}$–Au NPs probe allowed us to detect $Pb^{2+}$ in the presence of $H_2O_2$ (100 μM). We tested the sensitivity of the 4-MB/$S_2O_3^{2-}$–Au NPs probe for $Pb^{2+}$ ions in the solution with/without containing 100 μM $H_2O_2$. They provided same values of LOD (0.2 nM) and linear range (0.5–10 nM) (Fig. 2B and Fig. S2). On the other hand, the sensitivity of the 2-ME/$S_2O_3^{2-}$–Au NPs probe for $Pb^{2+}$ ions in the solution with/without containing 100 μM $H_2O_2$ were quite different; LODs were 20 and 0.5 nM, respectively [27].

### 3.5. Applications

To test the practicality of our developed approach, we used our 4-MB/$S_2O_3^{2-}$–Au NPs probe to determine the concentrations of $Pb^{2+}$ in river water from the National Taiwan Ocean University (NTOU) campus (Fig. 4A), in Montana Soil (SRM 2710; Fig. 4B) and urine (SRM 2672a; Fig. 4C) samples. We obtained a linear correlation ($R^2$ = 0.96) between the response and the concentration of $Pb^{2+}$ ions spiked into the river water (diluted twofold) over the range from 0.5 to 25 nM. Neither our sensing approach nor an ICP-MS-based system detected the presence of $Pb^{2+}$ ions in the river water

**Table 1**
Nanoparticles- and oligonucleotides-based optical assays for the detection of $Pb^{2+}$.

| Technique | Method | Probe unit | LOD; linear range | Real sample | Ref. |
|---|---|---|---|---|---|
| Scattering | Aggregation of Au NPs | 11-MUA–Au NPs[a] | N/A[b]; 0–200 μM | N/A[b] | [42] |
| Colorimetric | Disassembly of Au NPs | DNAzyme[c]/Au NPs | N/A[b]; 0.1–2 μM | N/A[b] | [44] |
| Colorimetric | ssDNA stronger protected Au NPs | DNAzyme and Au NPs | 500 nM; N/A[b] | N/A[b] | [45] |
| Colorimetric | ssDNA stronger protected Au NPs | DNAzyme and Au NPs | 3 nM; 3–100 nM | N/A[b] | [46] |
| Colorimetric | Aggregation of Au NPs | gallic acid–Au or Ag NPs | N/A[b]; 30–300 μM | N/A[b] | [40] |
| Colorimetric | Aggregation of Au NPs | gallic acid–Au NPs | 10 nM; 10–1000 nM | N/A[b] | [41] |
| Colorimetric | Leaching of Au NPs | 2-ME/$S_2O_3^{2-}$–Au NPs | 0.5 nM; 2.5 nM–10 μM | River and soil | [27] |
| Fluorescent | Chelation-enhanced fluorescence | BODIPY-magnetic $SiO_2$ NPs[d] | ~70 nM; N/A[b] | Removal of $Pb^{2+}$ from blood | [9] |
| Fluorescent | Quenching of fluorescence | Metalloprotein-QDs[e] | 5 nM; 5 nM–1 μM | Red blood cell | [23] |
| Fluorescent | FRET[f] | DNAzyme-catalytic beacon[g] | 20 nM; 0–500 nM | N/A[b] | [16] |
| Fluorescent | FRET[f] | unimolecular DNAzyme beacon | 3 nM; 2 nM–20 μM | N/A[b] | [15] |
| Fluorescent | Release-enhanced fluorescence | ATMND[h]-DNAzyme | 4 nM; 0–1 μM | N/A[b] | [17] |
| Fluorescent | FRET[f] | TBA beacon[i] | 0.3 nM; 0.5–30 nM | Soil | [20] |
| Colorimetric/luminescent | Release-enhanced catalysis | DNAzymes/ABTS or luminol[j] | 10 nM; N/A[b] | N/A[b] | [18] |
| Colorimetric | Aggregation of Au NPs | 4-MB/$S_2O_3^{2-}$–Au NPs | 0.2 nM; 0.5–10 nM | River, soil and urine | This study |

[a] 11-mercaptoundecanoic acid modified gold nanoparticle.
[b] Not available.
[c] $Pb^{2+}$–dependent RNA-cleaving DNAzyme.
[d] 4,4-Difluoro-4-bora-3a,4adiaza-s-indacene (BODIPY)-functionalized magnetic silica nanoparticles.
[e] Flg-A3 peptide-functionalized InGaP.
[f] Fluorescence resonance energy transfer.
[g] 8–17E DNAzyme aptamer-functionalized babeled with donor and quencher.
[h] 2-Amino-5,6,7-trimethyl-1,8-naphthyridine.
[i] Thrombin-binding aptamer babeled with donor and quencher.
[j] $Pb^{2+}$-dependent cleaving DNAzyme conjugated with horseradish peroxidase (HRP)-mimicking DNAzyme.

sample. The LOD (S/N ratio = 3) of the 4-MB/$S_2O_3^{2-}$–Au NP probe for the $Pb^{2+}$ ions in this complicated matrix was ca. 0.3 nM. In these measurements, the 4-MB/$S_2O_3^{2-}$–Au NP probe provided recoveries of 96–103% of $Pb^{2+}$ ions. By applying standard addition methods to our new approach and to the ICP-MS-based analysis, we determined the concentrations of $Pb^{2+}$ ions in the Montana Soil sample (certified value: 5.53 mg/g) to be 5.69 (±0.22) and 5.45 (±0.38) mg/g ($n$ = 5), respectively. The Student's $t$-test and $F$-test values for the correlations between the two methods were 1.22 and 2.98, respectively (2.31 and 6.39, respectively, at a 95% confidence level), suggesting that the two methods did not provide significantly different results. We also determined the concentrations of $Pb^{2+}$ ions in the Urine sample (certified value: 232 nM) to be 208 (±31) and 229 (±25) nM ($n$ = 5) by 4-MB/$S_2O_3^{2-}$–Au NP probe and ICP-MS, respectively. The Student's $t$-test and $F$-test values for the correlations between the two methods were 1.16 and 1.54, respectively. These results reveal the practicality of using our 4-MB/$S_2O_3^{2-}$–Au NPs probe for the determination $Pb^{2+}$ ions in environmental and biological samples.

In comparison with other nanoparticles- and oligonucleotides-based optical methods (Table 1), our label-free colorimetry-based assay for $Pb^{2+}$ is relatively simple, cost-effective, selective and sensitive. Note that most other techniques require covalent conjugation of alkanethiol–ligands or thiolated-oligonucleotides to NPs or dye molecules to oligonucleotides. In addition these techniques are few applied to determination of $Pb^{2+}$ in real samples. Relative to our previous leaching-based 2-ME/$S_2O_3^{2-}$–Au NPs sensor [27], the present probe provided advantages of tunable dynamic ranges, better selectivity, and greater practicality.

## 4. Conclusions

We have devised a new assay for the sensitive and selective detection of $Pb^{2+}$ ions based on the formation of PbAu alloys on the surfaces of Au NPs, resulting in displacement of the ligand shell of the Au NPs. The changes in the SPR absorptions of Au NPs allowed us to readily detect $Pb^{2+}$ ions in aqueous solution. Under the optimal conditions, the 4-MB/$S_2O_3^{2-}$–Au NP probe was highly sensitive (LOD = 0.2 nM) and selective (by at least 100-fold over other metal ions) toward $Pb^{2+}$ ions, with a linear detection range from 0.5 to 10 nM. This approach abrogates the need for complicated chemosensors or sophisticated equipment. We validated the practicality of this method through the analyses of river, soil and urine samples. To the best of our knowledge, this paper describes the first example of the use of a controllable ligand shell of Au NPs for the detection of heavy metal ions. This simple, rapid, and cost-effective sensing system appears to hold great practicality for the detection of heavy metal ions in real samples.

## Acknowledgements

This study was supported by the National Science Council of Taiwan under contract 97-2113-M-019-001-MY2.

## Appendix A. Supplementary data

Supplementary data associated with this article can be found, in the online version, at doi:10.1016/j.talanta.2010.05.004.

## References

[1] M.R. Knecht, M. Sethi, Anal. Bioanal. Chem. 394 (2009) 33–46.
[2] H. Needleman, Annu. Rev. Med. 55 (2004) 209–222.
[3] J.S. Casas, J. Sordo, Lead: Chemistry, Analytical Aspects, Environmental Impact and Health Effects, Elsevier, Amsterdam, 2006.
[4] http://www.epa.gov/safewater/contamin ants/index.html (accessed March 2010).
[5] K.S. Subramanian, G.V. Iyengar, Fresenius J. Anal. Chem. 352 (1995) 232–235.
[6] H.L. Needleman, Human Lead Exposure, CRC Press, Boca Raton, FL, 1991.
[7] E.C. Banks, L.E. Ferretti, D.W. Shucard, Neurotoxicology 18 (1997) 237–281.
[8] L. Marbella, B. Serli-Mitasev, P. Basu, Angew. Chem. Int. Ed. 48 (2009) 3996–3998.
[9] H.Y. Lee, D.R. Bae, J.C. Park, H. Song, W.S. Han, J.H. Jung, Angew. Chem. Int. Ed. 48 (2009) 1–6.
[10] Q. He, E.W. Miller, A.P. Wong, C.J. Chang, J. Am. Chem. Soc. 128 (2006) 9316–9317.
[11] S. Deo, H.A. Godwin, J. Am. Chem. Soc. 122 (2000) 174–175.
[12] F. Zapata, A. Caballero, A. Espinosa, A. Tárraga, P. Molina, Org. Lett. 10 (2008) 41–44.
[13] F.-Y. Wu, S.W. Bae, J.-I. Hong, Tetrahedron Lett. 47 (2006) 8851–8854.
[14] K. Kavallieratos, J.M. Rosenberg, W.-Z. Chen, T. Ren, J. Am. Chem. Soc. 127 (2005) 6514–6515.
[15] H. Wang, Y. Kim, H. Liu, Z. Zhu, S. Bamrungsap, W. Tan, J. Am. Chem. Soc. 131 (2009) 8221–8226.
[16] N. Nagraj, J. Liu, S. Sterling, J. Wu, Y. Lu, Chem. Commun. (2009) 4103–4105.
[17] Y. Xiang, A. Tong, Y. Lu, J. Am. Chem. Soc. 131 (2009) 15352–15357.

[18] J. Elbaz, B. Shlyahovsky, I. Willner, Chem. Commun. (2008) 1569–1571.
[19] J. Li, Y. Lu, J. Am. Chem. Soc. 122 (2000) 10466–10467.
[20] C.-W. Liu, C.-C. Huang, H.-T. Chang, Anal. Chem. 81 (2009) 2383–2387.
[21] P. Zuo, B.-C. Yin, B.-C. Ye, Biosens. Bioelectron. 25 (2009) 935–939.
[22] X.-G. Li, X.-L. Ma, M.-R. Huang, Talanta 78 (2009) 498–505.
[23] V.S. Shete, D.E. Benson, Biochemistry 48 (2009) 462–470.
[24] B.T. Farrer, V.L. Pecoraro, Curr. Opin. Drug Discov. Dev. 5 (2002) 937–943.
[25] A. Ivask, M. François, A. Kahru, H.-C. Dubourguier, M. Virta, F. Douay, Chemosphere 55 (2004) 147–156.
[26] T.-J. Lin, M.-F. Chung, Sensors 8 (2008) 582–593.
[27] Y.-Y. Chen, H.-T. Chang, Y.-C. Shiang, Y.-L. Hung, C.-K. Chiang, C.-C. Huang, Anal. Chem. 81 (2009) 9433–9439.
[28] K.P. Prathish, D. James, J. Jaisy, T.P. Rao, Anal. Chim. Acta 647 (2009) 84–89.
[29] E. Ranyuk, C.M. Douaihy, A. Bessmertnykh, F. Denat, A. Averin, I. Beletskaya, R. Guilard, Org. Lett. 11 (2009) 987–990.
[30] M. Hu, J. Chen, Z.-Y. Li, L. Au, G.V. Hartland, X. Li, M. Marquez, Y. Xia, Chem. Soc. Rev. 35 (2006) 1084–1094.
[31] M.E. Stewart, C.R. Anderton, L.B. Thompson, J. Maria, S.K. Gray, J.A. Rogers, R.G. Nuzzo, Chem. Rev. 108 (2008) 494–521.
[32] N.L. Rosi, C.A. Mirkin, Chem. Rev. 105 (2005) 1547–1562.
[33] R. Wilson, Chem. Soc. Rev. 37 (2008) 2028–2045.
[34] V. Myroshnychenko, J. Rodríguez-Fernández, I. Pastoriza-Santos, A.M. Funston, C. Novo, P. Mulvaney, L.M. Liz-Marzán, F.J.G. de Abajo, Chem. Soc. Rev. 37 (2008) 1792–1805.
[35] W. Zhao, M.A. Brook, Y. Li, ChemBioChem 9 (2008) 2363–2371.
[36] C.D. Medley, J.E. Smith, Z. Tang, Y. Wu, S. Bamrungsap, W. Tan, Anal. Chem. 80 (2008) 1067–1072.
[37] G.K. Darbha, A.K. Singh, U.S. Rai, E. Yu, H. Yu, P.C. Ray, J. Am. Chem. Soc. 130 (2008) 8038–8043.
[38] D. Li, A. Wieckowska, I. Willner, Angew. Chem. Int. Ed. 47 (2008) 3927–3931.
[39] C.A. Mirkin, R.L. Letsinger, R.C. Mucic, J.J. Storhoff, Nature 382 (1996) 607–609.
[40] K. Yoosaf, B.I. Ipe, C.H. Suresh, K.G. Thomas, J. Phys. Chem. C 111 (2007) 12839–12847.
[41] K.-W. Huang, C.-J. Yu, W.-L. Tseng, Biosens. Bioelectron. 25 (2010) 984–989.
[42] Y. Kim, R.C. Johnson, J.T. Hupp, Nano Lett. 1 (2001) 165–167.
[43] J.M. Slocik, J.S. Zabinski Jr., D.M. Phillips, R.R. Naik, Small 4 (2008) 548–551.
[44] J. Liu, Y. Lu, J. Am. Chem. Soc. 127 (2005) 12677–12683.
[45] H. Wei, B. Li, J. Li, S. Dong, E. Wang, Nanotechnology 19 (2008) 095501.
[46] Z. Wang, J.H. Lee, Y. Lu, Adv. Mater. 20 (2008) 3263–3267.
[47] J. Turkevich, Gold Bull. 18 (1985) 86–91.
[48] Test Methods for Evaluating Solid Waste, Physical/Chemical Methods, U. S. EPA SW-846, 3rd ed., U.S. Government Printing Office, Washington, DC, 1996.
[49] E.M.L. Lorentzen, H.M. Kingston, Anal. Chem. 68 (1996) 4316–4320.
[50] D. Feng, J.S.J. van Deventer, Hydrometallurgy 64 (2002) 231–246.
[51] G. Senanayake, Hydrometallurgy 90 (2008) 46–73.
[52] J.M. Chimenos, M. Segarra, L. Guzman, A. Karagueorgueva, F. Espiell, Hydrometallurgy 44 (1997) 269–286.
[53] J.D.E. Mclntyre, W.F. Peck Jr., J. Electrochem. Soc. 123 (1976) 1800–1813.
[54] R.F. Sandenbergh, J.D. Miller, Miner. Eng. 14 (2001) 1379–1386.
[55] G. Deschenes, R. Lastra, J.R. Brown, S. Jin, O. May, E. Ghali, Miner. Eng. 13 (2000) 1263–1279.
[56] R.A. Bryce, J.M. Charnock, R.A.D. Pattrick, A.R. Lennie, J. Phys. Chem. A 107 (2003) 2516–2523.
[57] T.-C. Chiu, L.-S. Huang, P.-C. Lin, Y.-C. Chen, Y.-J. Chen, C.-C. Lin, H.-T. Chang, Recent Pat. Nanotechnol. 1 (2007) 99–111.
[58] P.J. Renders, T.M. Seward, Geochim. Cosmochim. Acta 53 (1989) 245–253.